Artificial Intelligence Based Short-Term Motions Forecasting for Autonomous Marine Vehicles Control

J M Walker, MEng, MIEEE[a], Prof. A Coraddu[a*], Ph.D, MIMarEST, MIEEE, Ir. V Garofano[a], MEng, Prof. L Oneto[b], Ph.D, MIEEE

[a]*Delft University of Technology, Delft, Netherlands;* [b]*University of Genoa, Genoa, Italy*

*Corresponding author. Email: a.coraddu@tudelft.nl

Synopsis

The development of fast and accurate intelligent vessel control systems is a necessary milestone on the path toward operating autonomous marine vehicles effectively in harsh environments and complex mission settings. One of the main problems of existing control systems is the disparity between the forecasted behavior and how the vessel actually responds to its environment. This disparity can be partly attributed to the dependency on physics-based methods to model the response of the vessel and the fact that accurate high-fidelity physical models are too computationally expensive to be utilized in real time. One promising solution to this problem is to integrate the dynamic environmental conditions such as sea states, winds, and currents to model the response of the vessel. However, this may not be feasible with the existing physics-based controller strategies due to the high computational requirements. Instead, we propose using Artificial Intelligence (AI) based methods, which leverage Data Mining and Machine Learning, to enable fast and accurate short-term motions forecasting for autonomous marine vehicles. The AI-based approach is extremely time-aware in the forecasting phase since it does not rely on solving the physics behind the phenomenon but rather learns a phenomenon from historical examples linking the vessel's motions to a holistic view of its real-time environment. To test our hypothesis, we will develop state-of-the-art AI-based models for the short-term motions forecasting of the roll and trim of a twin-engine commercial vessel using real-world operational data and leverage statistical methods to validate our results.

Keywords: Autonomous Marine Vehicles (AMVs); Intelligent Control; State Prediction; Artificial Intelligence; Short-Term Motions Forecasting

1 Introduction

Autonomous Marine Vehicles (AMVs) are suggested as an integral step toward the reduction of emissions from shipping, the reduction of fatigue of seafarers, and increased safety measures at sea (Li and Fung, 2019). However, the deployment of fully autonomous vessels in a variety of complex mission settings remains a challenging task (Jokioinen et al., 2016; Thombre et al., 2022). The International Maritime Organization (IMO) has identified the required autonomy levels of maritime autonomous surface ships (International Maritime Organization, 2018) which is discussed at length in (Wang et al., 2019) along with a description of state-of-the-art research on motion control of Maritime Autonomous Surface Ships. In general, for a ship to be classified as fully autonomous, the vessel control system must be able to decide the best course of action itself. Therefore, before fully AMVs can be deployed, an effort must be made to develop intelligent control systems. While many motion control systems are available in the literature (Qi et al., 2015), there is still a significant amount of work to be done to tackle the existing disparity between the predicted behavior and how the vessel actually responds to its environment (Skulstad et al., 2021).

To understand the behavior and dynamics of an AMV in six Degrees of Freedom (DoF), we can leverage state-of-the-art models such as in Fossen and Smogeli (2004), which account for the three translational motions (surge, sway, and heave) and the three rotational motions (roll, pitch, and yaw). The real-time solution of numerical models such as in Fossen and Smogeli (2004) are fundamental for intelligent control systems to forecast the vessel state,

Authors' Biographies

Jake M Walker is a PhD candidate in the Department of Maritime and Transport Technology at Delft University of Technology where his primary focus is the development of Artificial Intelligence based solutions to the design and optimization of hull forms. He received his MEng in Mechanical Engineering from the University of Strathclyde in 2020 and has a keen interest in the application of Artificial Intelligence to address problems facing the maritime industry.

Prof. Andrea Coraddu is an Assistant Professor in the Department of Maritime and Transport Technology at Delft University of Technology and a visiting Professor at the University of Strathclyde. In 2012 he was awarded a Laurea and a PhD in Naval Architecture and Marine Engineering at the University of Genoa. His primary research involves taking advantage of on-board data availability in assessing vessel performance, energy optimization, and real-time monitoring of the primary systems towards autonomous operations.

Ir. Vittorio Garofano is a Research Engineer and coordinator of the technical activities at the ResearchLab Autonomous Shipping (RAS) in the Department of Maritime and Transport Technology at Delft University of Technology. His research interests include the implementation of vessel control algorithms with a focus on autonomous inland navigation, the software-hardware integration, and the design of robust control strategies.

Prof. Luca Oneto was born in Rapallo, Italy in 1986. He received his MSc in Electronic Engineering at the University of Genoa, Italy in 2010 and his PhD with the thesis "Learning Based On Empirical Data" in 2014. In 2017 he obtained the Italian National Scientific Qualification for the role of Associate Professor in Computer Engineering and in 2018 the one in Computer Science. He is currently an Assistant Professor in Computer Engineering at the University of Genoa with particular interests in Statistical Learning Theory and Data Science.

account for the external disturbances, and prescribe the optimal force allocations necessary to fulfill the mission criteria. For example, AMVs are often required to operate in harsh environments and complex mission settings, such as closed proximity and dense environments, station keeping, mooring, automatic docking, and helicopter operations.

Regardless of the application, a key part of intelligent control systems is real-time state prediction. Within the AMV control system, the role of state prediction is to accurately forecast the future state of the vessel at a large enough horizon to prescribe the optimal force allocations. For AMVs, the development of accurate state predictors will substantially reduce positional uncertainty in the control system and enable automatic control protocols, e.g., model predictive control (Skulstad et al., 2021). Existing control systems often rely on observers and state predictors, e.g., the Kalman Filter (De Masi et al., 2012). However, there are often some issues with the real-time implementation of current devices, such as a disparity between the real and forecasted motion due to simplified models to describe the vessel or its environment.

To overcome this disparity, we can leverage data from modern sensory technology in combination with automatic control systems to improve autonomous operations, evaluate the feasibility of potential missions, and identify the best control strategies to ensure the mission is completed successfully. The attention of this paper is focused on state prediction, as this is a critical aspect of developing intelligent control strategies and realizing the potential of fully autonomous marine vehicles.

2 Related Work

Solving the equation of motions of an AMV (Fossen and Smogeli, 2004) with Physical Models (PMs) often yields highly accurate results (Wang et al., 2019). However, obtaining fast and accurate state prediction using PMs is not a computationally trivial task, and often control strategies using PMs are developed upon many assumptions and simplifications of the underlying phenomena, so they can be implemented in real time.

On the other hand, we can use Artificial Intelligence (AI)-based methods, which leverage Data Mining and Machine Learning, to enable fast and accurate short-term motions forecasting. The crux of the AI-based approach is that we learn a phenomenon from historical examples (in contrast to PMs which rely on solving the physics behind the behavior). This means that we can leverage the AI-based approach with historical operational data to create complex models that can learn the relationship between the vessel motions and the real-time environment. Although AI-based methods can be quite computationally expensive during the model creation phase, they are highly accurate and computationally inexpensive during the forecasting phase, which is considered crucial for real-time and control applications (Coraddu et al., 2021). Considering that modern ships are an effective data center and capture a wide array of exogenous (the surrounding environment) and endogenous (on-board) features Coraddu et al. (2022), it is logical to exploit operational data for the purpose of a state prediction algorithm to enable intelligent control systems. In the rest of this section, we summarize the related work for marine state prediction algorithms.

In Rath and Subudhi (2020), the authors develop a state prediction algorithm for an AMV using extreme learning machines and tested models for pitch, pitch rate, heave, and heave velocity for an underwater vehicle. The model framework was a Nonlinear AutoRegressive Moving Average with eXogenous input (NARMAX) and could forecast their chosen KPIs over short periods. The data sample period is 0.56s, and the results indicate a reasonable performance with a time delay under 1s.

In De Masi et al. (2012), the authors develop a model for heave motion forecasting with reasonable performance and a forecast horizon of 15-30s RMSE$\sim 0.05-0.2\ [m]$. Furthermore, pitch and roll motion forecasting was carried out up to a 50s horizon with a hybrid NAR+wavelets framework, resulting in model accuracy of RMSE$\sim 0.05\ [^\circ]$ for pitch and RMSE$\sim 0.13\ [^\circ]$ for roll. Although very promising, these results were obtained from an extremely small data set (650 samples) and only describe the motions of an inertial platform over 1 day.

In Suhermi et al. (2018), the roll motion of a floating production unit was forecasted using an Autoregressive Integrated Moving Average (ARIMA) deep learning model. Synthetic data captured at very high frequency (15 Hz) was leveraged, and a hybrid model with a forecast of between 3s - 16s led to an RMSE$\sim 0.04\ [^\circ]$.

Finally, in Zhang and Liu (2014), the heading angle was forecasted with a horizon of 1s leading to an RMSE$\sim 0.2\ [^\circ]$, the extension of the horizon to 3s led to an RMSE$\sim 0.37\ [^\circ]$.

To summarize the current literature, it is worth mentioning that many articles focus on forecasting either the motions independent of the environment (Rath and Subudhi, 2020; De Masi et al., 2012; Suhermi et al., 2018; Zhang and Liu, 2014) or forecasting the environmental conditions and then inferring the motion (Krishna Kumar et al., 2019). Instead, we propose to couple the relationship between the ship and its operating conditions by enhancing the ship motion forecasting with the available environmental data. In addition, most of the work in the existing body of literature leverages synthetic data or scenarios to test the proposed hypotheses. Although this is a reasonable preliminary step, the use of synthetic data or limited scenarios does not contain the real-world noise and conditions that are essential to infer the true performance of the proposed algorithms. Therefore, it is fair to

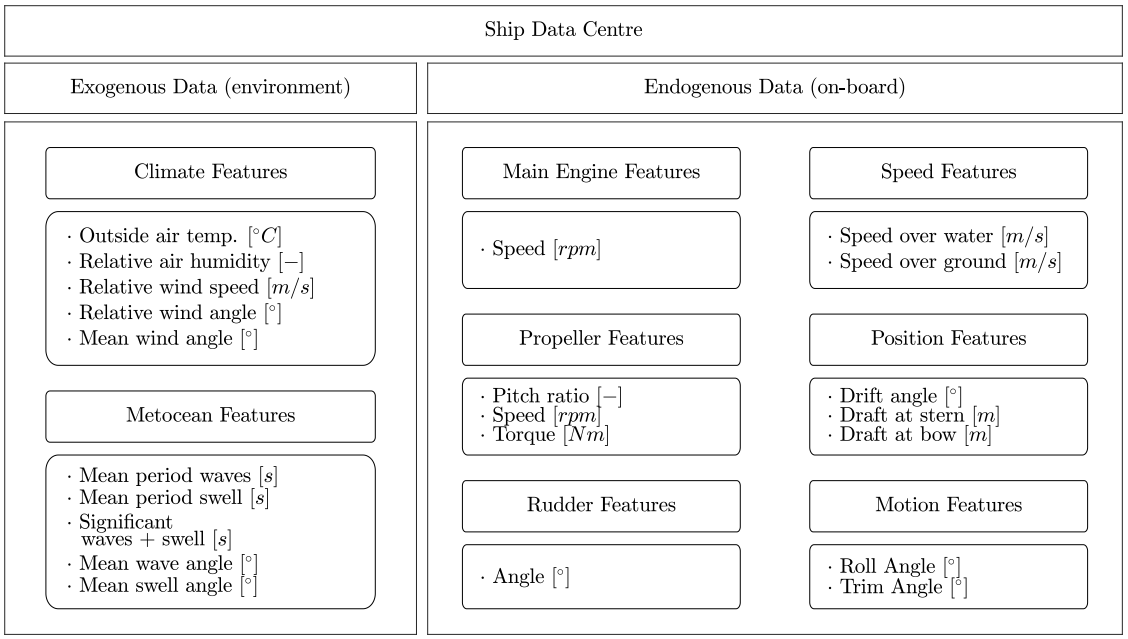

Figure 1: Pictoral representation of the data set which shows the categories of data coming from the ship data center and the available features.

consider that vessel state prediction using AI-based methods is still an emerging area of research and worthy of further exploration using real data and scenarios.

For the reasons outlined in Sections 1 – 2, the authors have decided to investigate the vessel state prediction problem from a perspective that couples the motion of the ship with its operating conditions. In this work, and in line with the available data (Section 3), the authors will investigate the Short-Term Motion Forecasting problem for the roll (φ) and trim (ψ) motions of a vessel using state-of-the-art AI-based methods. The roll motion (φ) results from the impact of environmental conditions acting with components perpendicular to the longitudinal axis, such as the force from waves and wind. It is also important to note, for many commercial vessels the moment of inertia of the vessel along its longitudinal axis is often much lower than along the other primary axes, which means particular attention should be given towards the stability along the longitudinal axis and the roll motion. On the other hand, the trim is the difference between the draft at the bow and stern of the vessel, and when these quantities are equal (i.e., $\psi = 0$ [°]) the ship is in the even keel position.

3 Dataset Description

In this work, we leverage real-world operational data gathered over a period of one year for a twin diesel engine commercial vessel. The original data set includes over $400,000$ samples, which are discontinuous (i.e., not all sampled in a continuous period), and sampled at inconsistent frequencies within the discontinuous sets. A pre-processing stage was carried out to address the inconsistent sampling and the data was re-sampled at a period of 3 [s] which reduced the data set to about 25% of the original size.

The data set (originating from the ship data center) contains the necessary information to complete the aim of this paper, which is to learn the complex relationship between the ship and its environment for short-term motions forecasting. The available features in the data set can be grouped into two categories: i) data exogenous to the vessel, which describes the environmental conditions, including the climate and metocean features; ii) data endogenous to the vessel, which describes the on-board behavior, such as the state of the propulsive system, the current position, and trajectory of the ship. We are interested in forecasting the vessel motions, i.e., the roll (φ) and the trim (ψ), which is a subset of the on-board data. The data set is represented pictorially in Figure 1 which shows the categories of data coming from the ship data center and the available features. Figure 2 instead shows selected histograms of relative frequency for climate features Figures 2a–2b, metocean features Figures 2c–2d, on-board features Figures 2e–2f, and the ship motions Figures 2g–2h. The data has been normalized to protect sensitive information.

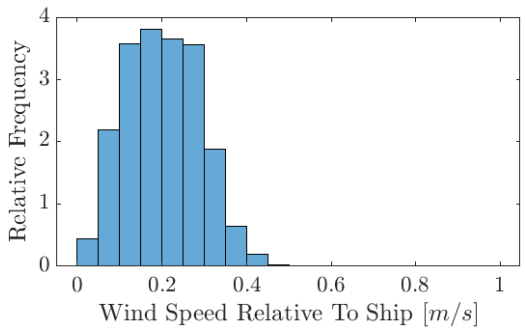

(a) Histogram of relative frequencies of the Wind Speed

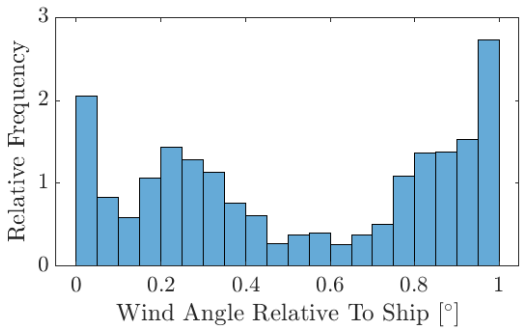

(b) Histogram of relative frequencies of the Wind Angle

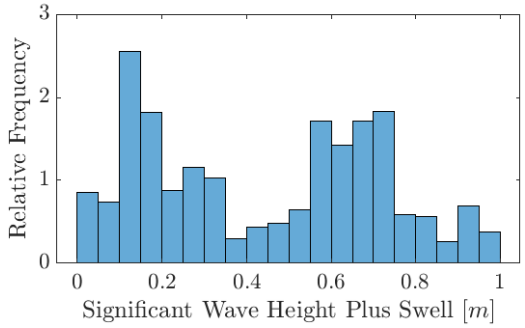

(c) Histogram of frequencies of the Wave Height + Swell

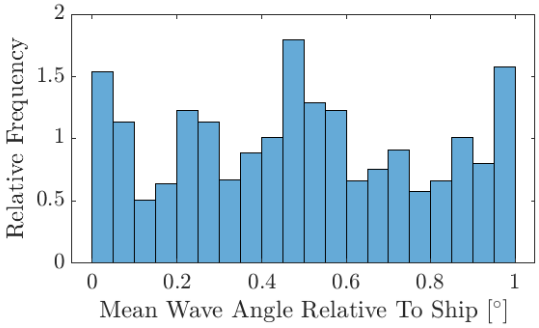

(d) Histogram of frequencies of the Mean Wave Angle

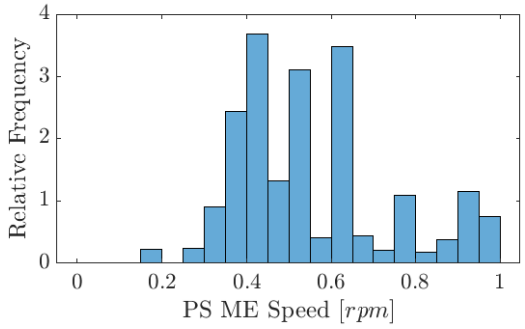

(e) Histogram of frequencies of the Port Side (PS) Main Engine (ME) Speed

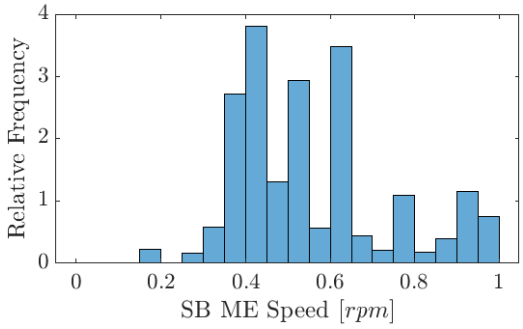

(f) Histogram of frequencies of the Starboard Side (SB) Main Engine (ME) Speed

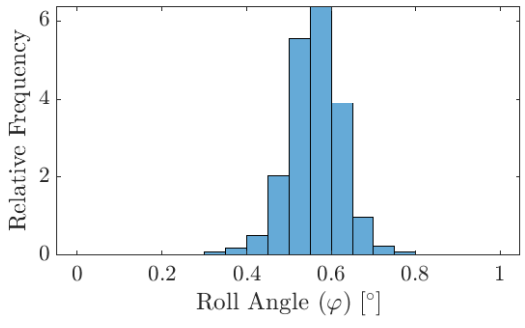

(g) Histogram of frequencies of the Roll Angle

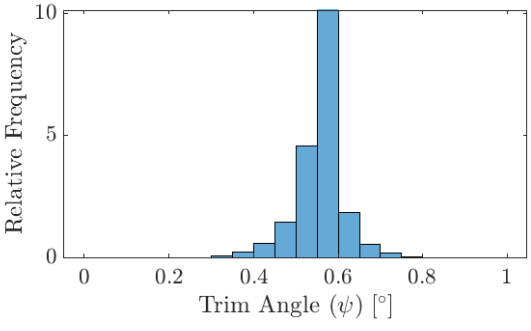

(h) Histogram of frequencies of the Trim Angle

Figure 2: Selected histograms of relative frequency for climate features (a)–(b), metocean features (c)–(d), onboard features (e)–(f), and the ship motions (g)–(h). The data has been normalized to protect sensitive information.

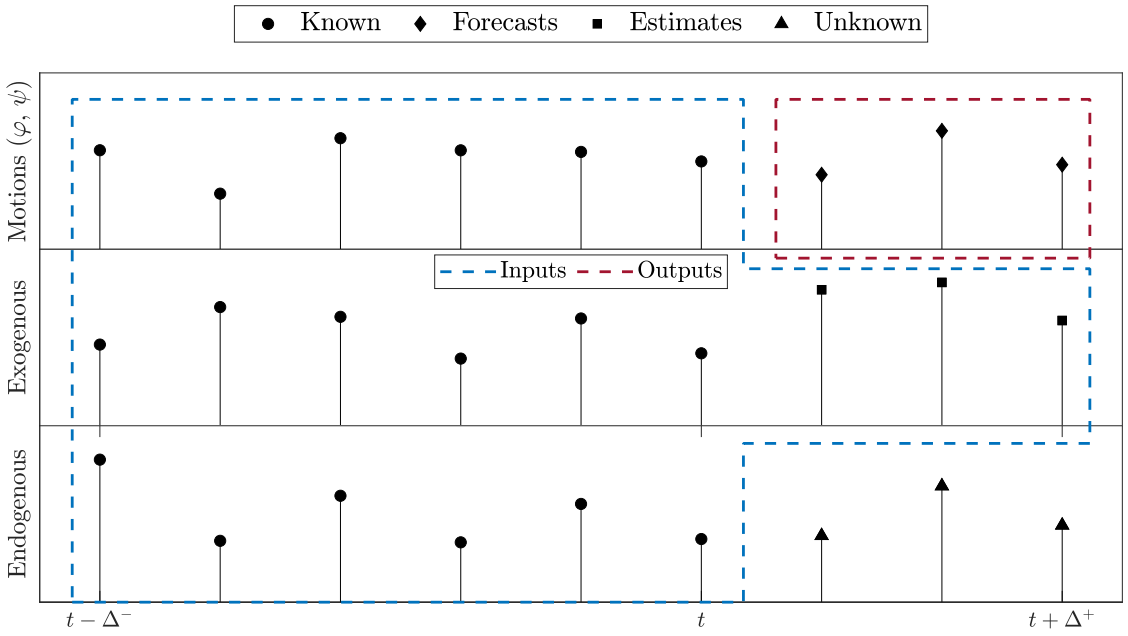

Figure 3: The short-term motions forecasting framework with the window of historical data in the period $[t-\Delta^-,t]$, the forecast horizon(s) up to $t+\Delta^+$, and estimations of some features during the period $(t,t+\Delta^+]$.

4 Method

The modelization in this paper begins with a general framework characterized by an input space $\mathscr{X} \subseteq \mathbb{R}^d$, an output space $\mathscr{Y} \subseteq \mathbb{R}^b$, and a phenomenon $\mu : \mathscr{X} \to \mathscr{Y}$ we would like to learn (Shalev-Shwartz and Ben-David, 2014; Hamilton, 1994). For the problem of pointwise motions prediction, $\mathscr{X}$ is composed by the exogeonous data describing the operating conditions of the vessel (i.e., the climate and metocean features according to Figure 1) and the endogenous data excluding the motions (i.e., the main engine, propeller, rudder, speed, and position features according to Figure 1), while the output space $\mathscr{Y}$ refers exclusively to the motions of the vessel (φ and ψ).

For the problem of short-term motions forecasting, we have to extend the above framework and introduce two model hyperparameters that govern the influence of time on the model. The first hyperparameter, Δ^-, represents the duration of historical data we include in the model, so the input space is now composed of past information during the time frame $[t-\Delta^-,t]$ (i.e., $[\mathscr{X},\mathscr{Y}] \subseteq \mathbb{R}^{d+b}$). The second hyperparameter, Δ^+, represents the prediction horizon, so the output space is now defined as the vessel motion (i.e., φ and ψ) at time $t+\Delta^+$. Furthermore, in the case where we can obtain a reliable estimation of some features, we can enhance the input space during the period $(t,t+\Delta^+]$. For the vessel motion problem, to improve the coupling between the vessel motion and its environment, we can introduce estimated environmental variables at the forecasted horizon. The described short-term motions forecasting framework with the window of historical data in the period $[t-\Delta^-,t]$, the forecast horizon(s) up to $t+\Delta^+$, and estimations of some features during the period $(t,t+\Delta^+]$ is shown in Figure 3. The model hyperparameter Δ^- must be considered carefully to balance its influence over the model. Since increasing Δ^- (and saturating the model with historical data) suffers from the curse of dimensionality, while shrinking Δ^- (and not adequately capturing dynamic effects) restricts our ability to forecast accurately (Shalev-Shwartz and Ben-David, 2014; Oneto, 2020; Hamilton, 1994). Instead, the optimal Δ^+ depends on the application: clearly the deeper into the future we are able to forecast the better, but generally the prediction accuracy will decrease as the time horizon is extended (Shalev-Shwartz and Ben-David, 2014; Hamilton, 1994; Oneto, 2020). For what concerns the problem at hand, a reliable Δ^+ forecast of 10–60 [s] for the motions state-prediction will provide the vessel control system with adequate time to perform the thrust allocation procedure.

In this paper, the model f, will be developed using state-of-the-art AI-based techniques for the reasons described in Section 2. We use a machine learning framework to map the problem of short-term motions forecasting into a conventional regression one (Vapnik, 1998). The machine learning framework allows us to exploit an algorithm $\mathscr{A}_{\mathscr{H}}$ to learn f (which is the best approximation of μ) where the set of possible hyperparameters $\mathscr{H}$ determines the generalization performance of $\mathscr{A}$ (Oneto, 2020). The information to learn the model f is encompassed within the data set, characterized by n historical examples, and where $\mathscr{D}_n = \{(x_1,y_1),\cdots,(x_n,y_n)\}$ with $x \in \mathscr{X}$ and $y \in \mathscr{Y}$.

Learning a model for the AI-based approach in this paper starts by minimizing a cost function which considers the trade-off between the accuracy on the training data and the complexity of the learned model (Vovk, 2013). The

best model f^* is chosen as the one that is complicated enough to learn from the data without succumbing to the overfitting tendency

$$f^*: \quad \min_f \quad \hat{L}_n(f) + \lambda\, C(f). \tag{1}$$

The contribution from the empirical error $\hat{L}_n(f)$ is for fitting the model to the data (Shawe-Taylor and Cristianini, 2004), and the complexity measure $C(\cdot)$ is to avoid the overfitting tendency by regulating the complexity of the solution. Instead, the hyperparameter $\lambda \in [0,\infty)$ is the penalty on the complexity. Finding the optimal value for λ is an important task (as explained later in this section) and dependent on the problem at hand.

Regarding the choice of the learning algorithm to build the model f, there are a number of families of algorithms that we could leverage for this problem, i.e., kernel methods (Shawe-Taylor and Cristianini, 2004), neural networks (Goodfellow et al., 2016), or random forests (Breiman, 2001). In fact, it is not possible to determine *a-priori* which algorithm will perform best or shortcut a rigorous model selection process (Shalev-Shwartz and Ben-David, 2014). Therefore, for the AI-based approach to short-term vessel motions forecasting, we have elected to use an algorithm from the family of kernel methods called Kernel Regularised Least Squares (KRLS) (Vovk, 2013) since it is a state-of-the art learning method. In KRLS, models are defined as

$$f(x) = w^T \phi(x), \tag{2}$$

where ϕ is an a-priori defined feature mapping (Shalev-Shwartz and Ben-David, 2014) allowing to keep the structure of $f(x)$ linear. In KRLS, we chose the square loss to measure the empirical error

$$\hat{L}_n(f) = \sum_{i=1}^{n} [f(x_i) - y_i]^2, \tag{3}$$

and the complexity of models are measured as

$$C(f) = \|w\|^2, \tag{4}$$

Consequently, Problem (1) can be reformulated as

$$w^*: \quad \min_w \quad \sum_{i=1}^{n} \left[w^T \phi(x_i) - y_i\right]^2 + \lambda \|w\|^2. \tag{5}$$

By exploiting the Representer Theorem (Scholkopf, 2001), the solution f^* of Problem (5) can be expressed as a linear combination of the samples projected in the space defined by ϕ

$$f^*(x) = \sum_{i=1}^{n} \alpha_i \phi(x_i)^T \phi(x). \tag{6}$$

The main idea behind KRLS is to reformulate the above problem by exploiting the kernel trick, which means we do not actually require an explicit knowledge of the feature mapping ϕ, thanks to the use of kernel functions $K(x_i,x) = \phi(x_i)^T \phi(x)$

$$f^*(x) = \sum_{i=1}^{n} \alpha_i K(x_i,x). \tag{7}$$

There are several kernel functions common in the literature (Vovk, 2013; Cristianini and Shawe-Taylor, 2000), but the Gaussian Kernel is often favored because it can implicitly map the data into an infinite dimensional space and consequently, the KRLS can learn any possible function (Shawe-Taylor and Cristianini, 2004). The Gaussian Kernel can be expressed as

$$K(x_i,x) = e^{-\gamma \|x_i - x\|^2}, \tag{8}$$

The kernel hyperparameter γ is responsible for regulating the non-linearity of the solution and must be tuned carefully (as explained later). Now Problem (5) can be reformulated by exploiting kernels as

$$\alpha^*: \quad \min_\alpha \quad \|Q\alpha - y\|^2 + \lambda\, \alpha^T Q \alpha, \tag{9}$$

where $y = [y_1,\ldots,y_n]^T$, $\alpha = [\alpha_1,\ldots,\alpha_n]^T$, the matrix Q corresponds such that $Q_{i,j} = K(x_j,x_i)$, and the identity matrix $I \in \mathbb{R}^{n\times n}$. By setting the gradient equal to zero w.r.t. α we find that it is possible to state

$$(Q + \lambda I)\, \alpha^* = y, \tag{10}$$

which is a linear system for which efficient solvers have been developed over the years Young (2003). However, if computational requirements are a concern, it is possible to regulate the computational complexity by sampling the training set.

At this point, the authors have defined how to build the model, but we still have to address the problem of how to select the best model from the set of candidate ones. To tackle this, we need to define a procedure to select the optimal set of hyperparameters (λ, γ, and Δ^-) and a method to estimate the performance of our final model. Model Selection (MS) and Error Estimation (EE) deal with exactly these challenges (Oneto, 2020). In this paper, we leverage resampling techniques to ensure statistically relevant results because they work well in most situations and tend to outperform other techniques in practice (Oneto, 2020). Resampling techniques are based on a simple idea: the original dataset $\mathscr{D}_n$ is resampled once or many (n_r) times, with or without replacement, to build three independent datasets called the learning, validation, and test sets, respectively $\mathscr{L}_l^r$, $\mathscr{V}_v^r$, and $\mathscr{T}_t^r$, with $r \in \{1, \cdots, n_r\}$ such that

$$\mathscr{L}_l^r \cap \mathscr{V}_v^r = \oslash, \quad \mathscr{L}_l^r \cap \mathscr{T}_t^r = \oslash, \quad \mathscr{V}_v^r \cap \mathscr{T}_t^r = \oslash \tag{11}$$

$$\mathscr{L}_l^r \cup \mathscr{V}_v^r \cup \mathscr{T}_t^r = \mathscr{D}_n \tag{12}$$

The role of the MS phase is to identify the best combination of hyperparameters $\mathscr{H} = \{\lambda, \gamma, \Delta^-\}$ out of the possible set $\mathfrak{H} = \{\mathscr{H}_1, \mathscr{H}_2, \cdots\}$ for the algorithm $\mathscr{A}_{\mathscr{H}}$ according to

$$\mathscr{H}^* : \quad \arg\min_{\mathscr{H} \in \mathfrak{H}} \sum_{r=1}^{n_r} M(\mathscr{A}_{\mathscr{H}}(\mathscr{L}_l^r), \mathscr{V}_v^r), \tag{13}$$

where each model $f = \mathscr{A}_{\mathscr{H}}(\mathscr{L}_l^r)$ is learned from the algorithm $\mathscr{A}$ with the hyperparameters $\mathscr{H}$ and the data $\mathscr{L}_l^r$, and the accuracy is evaluated according to the desired metric $M(f, \mathscr{V}_v^r)$. Since the data in $\mathscr{L}_l^r$ are independent from the data in $\mathscr{V}_v^r$, $\mathscr{H}^*$ should be the set of hyperparameters which corresponds to developing a model that can also perform well on data independent from the training set. The EE phase is to evaluate the performance of the optimal model $f_{\mathscr{A}}^* = \mathscr{A}_{\mathscr{H}^*}(\mathscr{D}_n)$ according to

$$M(f_{\mathscr{A}}^*) = \frac{1}{n_r} \sum_{r=1}^{n_r} M(\mathscr{A}_{\mathscr{H}^*}(\mathscr{L}_l^r \cup \mathscr{V}_v^r), \mathscr{T}_t^r). \tag{14}$$

Since the data in $\mathscr{L}_l^r \cup \mathscr{V}_v^r$ are independent from the ones in $\mathscr{T}_t^r$, $M(f_{\mathscr{A}}^*)$ is an unbiased estimator of the true performance, measured with the metric M, of the final model Oneto (2020). In this work we will rely on a Monte-Carlo resampling procedure with $n_r = 30$ and resampling without replacement (Oneto, 2020). It is important to stress that for this application, we must also abide by an additional constraint, which is the dependence in time between the samples. For this reason, when resampling the data from $\mathscr{D}_n$ we actually preserve the chronology in $\mathscr{L}_l^r$, $\mathscr{V}_v^r$, and $\mathscr{T}_t^r$ (Hamilton, 1994).

Finally, concerning the metric M that we will use in this work, we will rely on three error metrics to estimate the performance of the model on $\mathscr{T}_t^r = \{(x_1^r, y_1^r), \cdots, (x_t^r, y_t^r)\}$. The error metrics were selected to provide good insight into the performance of the models from a physical point of view, without burdening the reader with too many descriptions of the model quality. The Mean Absolute Error (MAE) which computes the average absolute loss of f over $\mathscr{T}_t^r$

$$\mathrm{MAE}(f) = \frac{1}{t} \sum_{i=1}^{t} |f(x_i^r) - y_i^r| \tag{15}$$

The Mean Absolute Percentage Error (MAPE) which computes the average absolute loss of f over $\mathscr{T}_t^r$ as a percentage

$$\mathrm{MAPE}(f) = \frac{100}{t} \sum_{i=1}^{t} \left| \frac{f(x_i^r) - y_i^r}{y_i^r} \right| \tag{16}$$

The Mean Square Error (MSE) is the average of the square loss of f over $\mathscr{T}_t^r$

$$\mathrm{MSE}(f) = \frac{1}{t} \sum_{i=1}^{t} (f(x_i^r) - y_i^r)^2 \tag{17}$$

Since in regression it is quite hard to synthesize the quality of a predictor in a single metric we will also rely on visualization techniques like the scatter plot of real vs. predicted values (Shao et al., 2017) in addition to the plot of the track in time.

Table 1: Selected error metrics when varying Δ^- and Δ^+ with optimal (λ, γ) for the short-term motions forecasting of the roll angle (φ). The statistically validated Mean Absolute Error (MAE), Mean Absolute Percentage Error (MAPE), and Mean Squared Error (MSE) metrics are reported at the original scale of the data alongside the interval of confidence evaluated from the t-student's distribution with $(n_r - 1)$ degrees of freedom. The optimal value for each metric, for each Δ^+, is reported in **bold**.

		Δ^- [s]				
		3	**15**	**30**	**45**	**60**
		Mean Absolute Error (MAE) [°]				
Δ^+ [s]	**3**	0.0442±0.0014	**0.0328±0.0011**	0.0337±0.0010	0.0343±0.0007	0.0342±0.0010
	6	0.0726±0.0019	0.0655±0.0025	**0.0646±0.0018**	0.0666±0.0017	0.0662±0.0022
	12	0.0861±0.0019	0.0853±0.0037	**0.0848±0.0026**	0.0874±0.0022	0.0861±0.0022
	24	0.1338±0.0033	0.1335±0.0029	**0.1302±0.0034**	0.1328±0.0029	0.1323±0.0032
	48	0.2120±0.0025	0.2038±0.0020	**0.1996±0.0035**	0.2036±0.0035	0.2030±0.0041
		Mean Absolute Percentage Error (MAPE) [%]				
Δ^+ [s]	**3**	0.0238±0.0022	**0.0202±0.0026**	0.0205±0.0042	0.0198±0.0045	0.0228±0.0037
	6	0.0426±0.0043	0.0418±0.0033	**0.0394±0.0050**	0.0416±0.0043	0.0396±0.0015
	12	0.0576±0.0058	0.0499±0.0034	**0.0474±0.0042**	0.0521±0.0040	0.0538±0.0032
	24	0.0800±0.0095	0.0843±0.0106	**0.0821±0.0095**	0.0813±0.0069	0.0808±0.0075
	48	0.1459±0.0092	0.1447±0.0172	0.1377±0.0097	**0.1361±0.0073**	0.1422±0.0105
		Mean Squared Error (MSE) [°^{2}]				
Δ^+ [s]	**3**	8.9e-03±6.2e-04	**4.5e-03±4.7e-04**	5.3e-03±1.2e-03	1.3e-02±1.2e-02	5.0e-03±6.4e-04
	6	2.1e-02±2.2e-03	3.7e-02±4.0e-02	**1.7e-02±2.8e-03**	1.7e-02±2.2e-03	1.6e-02±1.5e-03
	12	2.5e-02±2.2e-03	6.7e-02±8.0e-02	**2.5e-02±3.0e-03**	2.7e-02±6.0e-03	2.4e-02±2.2e-03
	24	5.1e-02±3.6e-03	1.0e-01±1.0e-01	**4.5e-02±4.2e-03**	4.6e-02±6.1e-03	4.5e-02±3.1e-03
	48	9.3e-02±2.8e-03	8.7e-02±1.1e-02	**7.8e-02±3.0e-03**	8.4e-02±4.5e-03	8.2e-02±3.8e-03

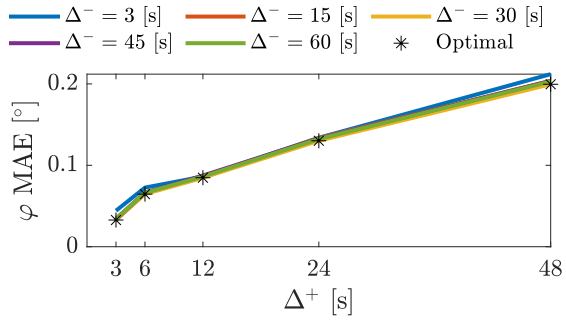

(a) The MAE [°] (lower is better) reported at the original scale of the data for the roll angle (φ) versus Δ^+ according to fixing Δ^- with optimal (λ, γ). The optimal Δ^- is the one that results in the lowest MAE for each Δ^+ which is indicated by $*$ in the figure.

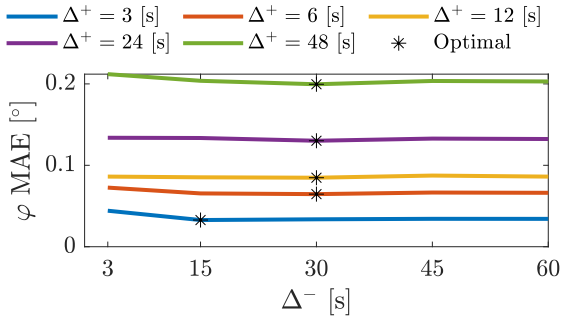

(b) The MAE [°] (lower is better) reported at the original scale of the data for the roll angle (φ) versus Δ^- according to fixing Δ^+ with optimal (λ, γ). The optimal Δ^- is the one that results in the lowest MAE for each Δ^+ which is indicated by $*$ in the figure.

Figure 4: The MAE [°] (lower is better) reported at the original scale of the data for the roll angle (φ) versus Δ^- and Δ^+ according to fixing the other Δ hyperparameter with optimal (λ, γ). The optimal Δ^- is the one that results in the lowest MAE for each Δ^+ which is indicated by $*$ in the figures.

Table 2: Selected error metrics when varying Δ^- and Δ^+ with optimal (λ, γ) for the short-term motions forecasting of the trim angle (ψ) respectively. The statistically validated Mean Absolute Error (MAE), Mean Absolute Percentage Error (MAPE), and Mean Squared Error (MSE) metrics are reported at the original scale of the data alongside the interval of confidence evaluated from the t-student's distribution with $(n_r - 1)$ degrees of freedom. The optimal value for each metric, for each Δ^+, is reported in **bold**.

		Δ^- [s]				
		3	**15**	**30**	**45**	**60**
		Mean Absolute Error (MAE) [°]				
Δ^+ [s]	**3**	0.0025±0.0001	**0.0020±0.0001**	0.0021±0.0001	0.0022±0.0001	0.0022±0.0001
	6	0.0026±0.0001	**0.0022±0.0001**	0.0022±0.0001	0.0023±0.0001	0.0023±0.0001
	12	0.0026±0.0001	**0.0024±0.0001**	0.0024±0.0001	0.0024±0.0001	0.0024±0.0001
	24	0.0028±0.0001	0.0027±0.0001	**0.0026±0.0001**	0.0026±0.0001	0.0026±0.0001
	48	0.0031±0.0001	0.0029±0.0001	**0.0028±0.0000**	0.0029±0.0001	0.0028±0.0001
		Mean Absolute Percentage Error (MAPE) [%]				
Δ^+ [s]	**3**	0.0008±0.0000	**0.0007±0.0001**	0.0007±0.0000	0.0008±0.0000	0.0008±0.0001
	6	0.0009±0.0000	**0.0008±0.0001**	0.0008±0.0001	0.0008±0.0001	0.0008±0.0001
	12	0.0009±0.0001	**0.0008±0.0001**	0.0008±0.0001	0.0009±0.0002	0.0008±0.0001
	24	0.0010±0.0001	**0.0009±0.0001**	0.0009±0.0001	0.0010±0.0001	0.0009±0.0001
	48	0.0010±0.0000	0.0010±0.0001	**0.0009±0.0001**	0.0010±0.0001	0.0011±0.0002
		Mean Squared Error (MSE) [°^{2}]				
Δ^+ [s]	**3**	4.1e-05±3.8e-06	**3.7e-05±4.5e-06**	4.1e-05±6.4e-06	3.6e-05±4.4e-06	3.6e-05±3.6e-06
	6	4.6e-05±2.7e-06	**3.9e-05±6.9e-06**	4.1e-05±5.9e-06	4.3e-05±7.2e-06	4.3e-05±4.7e-06
	12	4.3e-05±6.7e-06	4.3e-05±6.4e-06	**3.9e-05±6.5e-06**	4.4e-05±5.1e-06	4.1e-05±4.8e-06
	24	4.8e-05±4.1e-06	5.0e-05±4.7e-06	**4.6e-05±6.4e-06**	4.6e-05±4.5e-06	4.8e-05±5.5e-06
	48	5.2e-05±3.6e-06	4.8e-05±5.1e-06	**4.7e-05±3.9e-06**	5.3e-05±6.4e-06	5.1e-05±6.3e-06

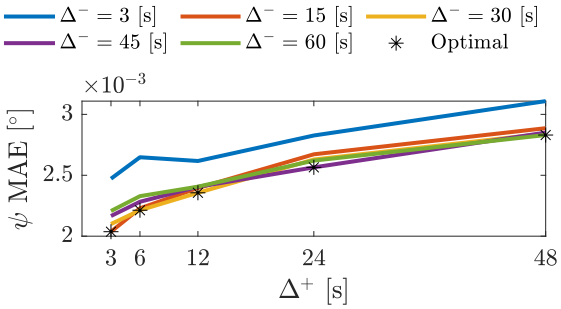

(a) The MAE [°] (lower is better) reported at the original scale of the data for the trim angle (ψ) versus Δ^+ according to fixing Δ^- with optimal (λ, γ). The optimal Δ^- is the one that results in the lowest MAE for each Δ^+ which is indicated by $*$ in the figure.

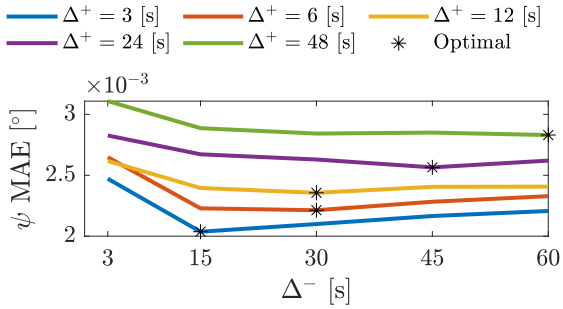

(b) The MAE [°] (lower is better) reported at the original scale of the data for the trim angle (ψ) versus Δ^- according to fixing Δ^+ with optimal (λ, γ). The optimal Δ^- is the one that results in the lowest MAE for each Δ^+ which is indicated by $*$ in the figure.

Figure 5: The MAE [°] (lower is better) reported at the original scale of the data for the trim angle (ψ) versus Δ^- and Δ^+ according to fixing the other Δ hyperparameter with optimal (λ, γ). The optimal Δ^- is the one that results in the lowest MAE for each Δ^+ which is indicated by $*$ in the figures.

5 Results

This section presents the results of the methodology described in Section 4 on the data described in Section 3. The set of hyperparameters investigated in this paper is $\mathscr{H} = \{\lambda, \gamma, \Delta^-\}$ where $\lambda \in \{10^{-6}, 10^{-5.8}, \cdots, 10^{4}\}$, $\gamma \in \{10^{-6}, 10^{-5.8}, \cdots, 10^{4}\}$, and $\Delta^- \in \{3, 15, 30, 45, 60\}$ [s]. The set of hyperparameter combinations was investigated using the grid search method, i.e., $\mathfrak{H} = \{10^{-6}, 10^{-5.8}, \cdots, 10^{4}\} \times \{10^{-6}, 10^{-5.8}, \cdots, 10^{4}\} \times \{3, 15, 30, 45, 60\}$. The set of Δ^+ horizons was chosen as $\{3, 6, 12, 24, 48\}$ [s] as this range will provide a good understanding of the performance of the models as the forecast horizon increases.

Tables 1 and 2 show the selected error metrics when varying Δ^- and Δ^+ with optimal (λ, γ) for the short-term motions forecasting of the roll angle (φ) and trim angle (ψ) respectively. The statistically validated Mean Absolute Error (MAE), Mean Absolute Percentage Error (MAPE), and Mean Squared Error (MSE) metrics are reported at the original scale of the data alongside the interval of confidence evaluated from the t-student's distribution at 95% confidence with $(n_r - 1)$ degrees of freedom. The optimal value for each metric, for each Δ^+, is reported in **bold**.

Figures 4 and 5 illustrate the MAE [°] (lower is better) reported at the original scale of the data for the roll angle (φ) and trim angle (ψ) respectively versus Δ^- and Δ^+ according to fixing the other Δ hyperparameter and with optimal (λ, γ). The optimal Δ^- is the one that results in the lowest MAE for each Δ^+ which is indicated by $*$ in the figures.

From Tables 1 and 2 and Figures 4 and 5 we can infer the best Δ^- out of the set of possible ones for each Δ^+ horizon and for each of the vessel motions. The general trend (for all of the metrics) in these tables suggests that the models for short-term motions forecasting were very sensitive to the influence of time through the hyperparameters Δ^- and Δ^+. It can be seen that an optimal period of historical data exists for each motion, and for each Δ^+ horizon, so that the models were not ambivalent to the previous motions, but also not saturated with too much historical behavior. According to each metric, the optimal Δ^- may vary, we have selected Δ^- according to the lowest MAE for further investigation.

After selecting the best value of Δ^- according to Tables 1 and 2 and Figures 4 and 5 the models were validated on previously unseen data for each Δ^+ horizon. Figure 6a – Figure 6j shows the short-term motions forecasting on previously unseen data for the roll (φ) and trim (ψ) angle for $\Delta^+ = \{3, 6, 12, 24, 48\}$ [s] and Δ^- fixed according to Tables 1 and 2. For each of the motions, each figure includes a portion of the track in time with the real and predicted motion, the histogram of frequencies for the real motion, a heatmap scatterplot of the real versus predicted values, and a histogram of the Absolute Percentage Error (APE) of the model. The values have been normalized to protect sensitive information.

According to Figure 6 there are several observations can be made from the results: i) as expected from the theory, and observing from Tables 1 and 2, an optimal value for Δ^- exists to provide enough information to accurately forecast the short-term motions; ii) as for the forecast horizon (Δ^+) the further we extend into the future, the less accurate our predictions become; and iii) there is a good agreement between the real and predicted short-term motions as reported in Figures 6a–6j, which demonstrates the models were effective at learning the short-term motions.

In summary, the results indicate that our framework for the AI-based short-term motions forecasting proved to be an effective strategy for operators to utilize in the case where a time-sensitive forecast of the vessel motion is required. For a small Δ^+, as one may expect, the errors are low (MAE for $\varphi \approx 0.033$ [°] and MAE for $\psi \approx 0.0020$ [°]). However, for the target application of intelligent control systems, we are interested in a horizon of $\Delta^+ \sim 24$–48 [s]. At the target horizon, the performance of the model is adequate to consider the use of AI-based state prediction in intelligent control systems (MAE for $\varphi \approx 0.13$–0.20 [°] and MAE for $\psi \approx 0.0026$–0.0028 [°]). Importantly, this work serves as a preliminary step to validate the presented framework on the limited available real operational data and further experiments in this field are recommended.

6 Conclusion

To conclude, the authors would like to reiterate that this work represents a preliminary step forward on the path toward developing reliable AI-based short-term motions forecasting for the intelligent control of AMVs. In this paper, we validated our short-term motion forecasting framework on a limited amount of real-world operational data from one vessel gathered over a period of one year. The results indicate that leveraging AI-based methods offer a promising insight into the behavior and dynamics of AMVs. For the required horizon of $\Delta^+ \sim 24$–48 [s], our results show the potential for AI-based models to be used for the state prediction within an intelligent control systems for an AMV. For this reason, we recommend a further study into the efficacy of AI-based short-term motions forecasting with a more extensive set of real world data and longer time frames to consider the forecasting of other AMV motions not included in this work. Finally, AI-based short-term motions forecasting models should be integrated into AMVs and deployed to validate the potentiality of the models.

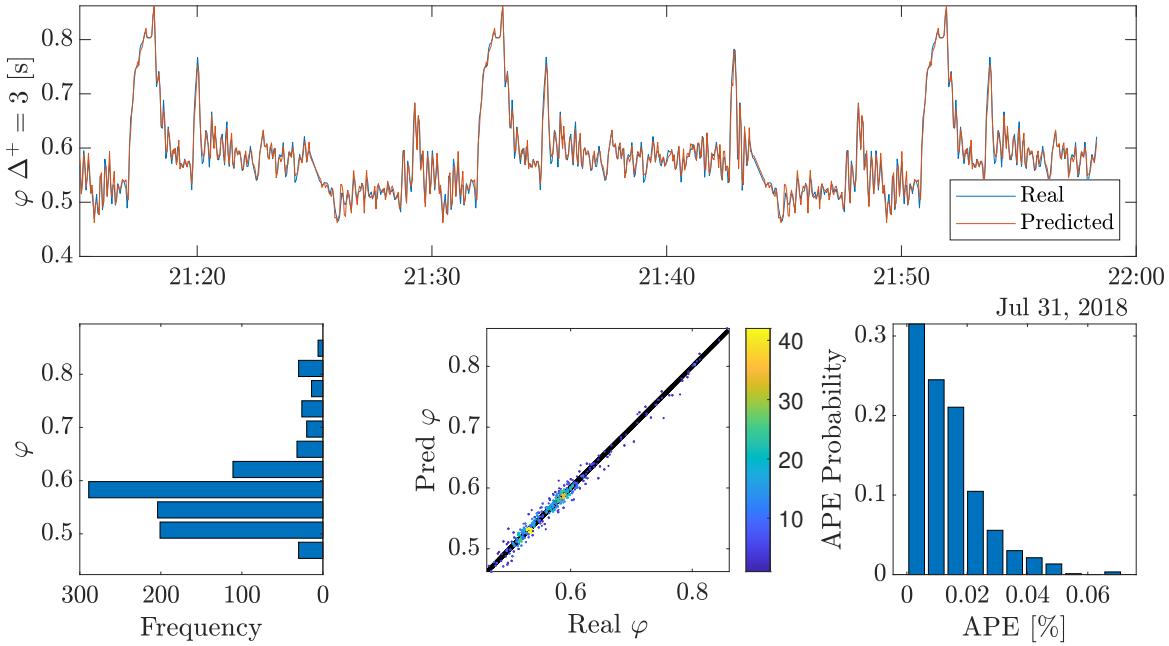

(a) The short-term motions forecasting for the roll (φ) angle for $\Delta^+ = 3$ [s] and $\Delta^- = 15$ [s] is fixed according to Table 1. The figure includes a portion of the track in time with the real and predicted motion, the histogram of frequencies for the real motion, a heatmap scatterplot of the real versus predicted values, and a histogram of the Absolute Percentage Error of the model.

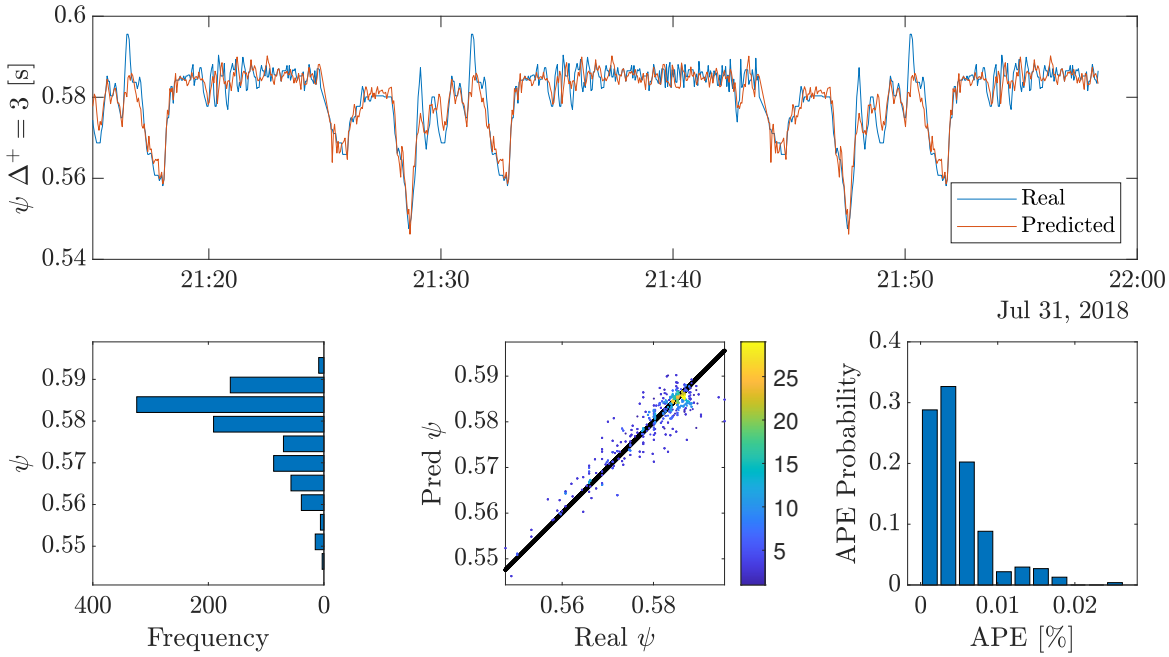

(b) The short-term motions forecasting for the trim (ψ) angle for $\Delta^+ = 3$ [s] and $\Delta^- = 15$ [s] is fixed according to Table 2. The figure includes a portion of the track in time with the real and predicted motion, the histogram of frequencies for the real motion, a heatmap scatterplot of the real versus predicted values, and a histogram of the Absolute Percentage Error of the model.

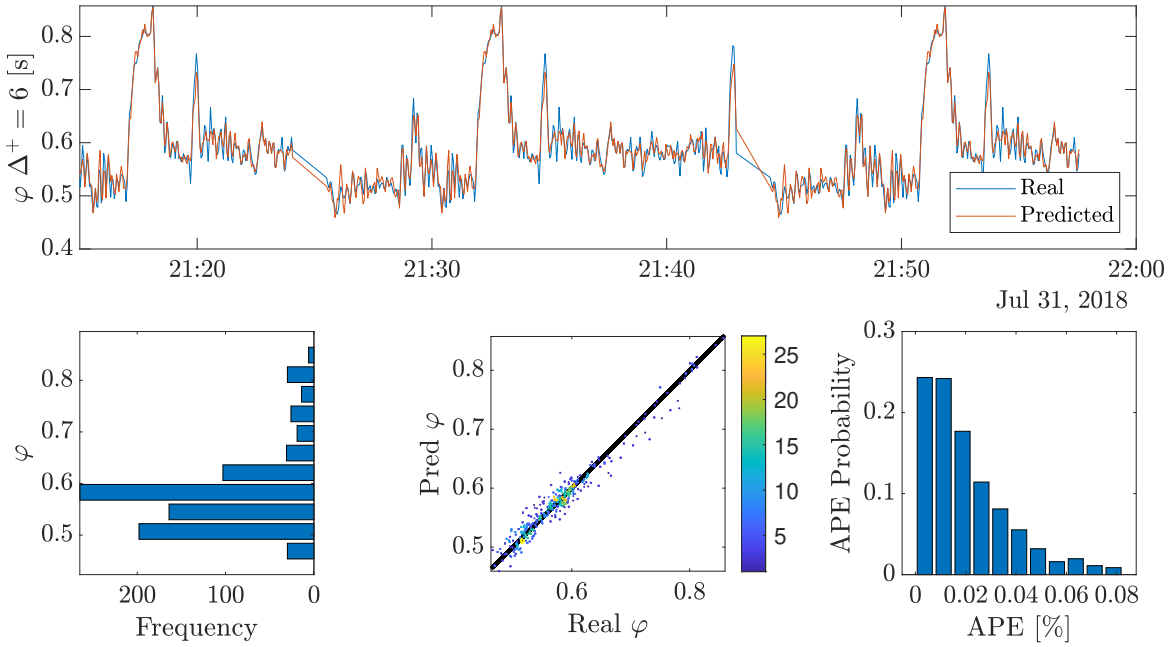

(c) The short-term motions forecasting for the roll (φ) angle for $\Delta^+ = 6$ [s] and $\Delta^- = 30$ [s] is fixed according to Table 1. The figure includes a portion of the track in time with the real and predicted motion, the histogram of frequencies for the real motion, a heatmap scatterplot of the real versus predicted values, and a histogram of the Absolute Percentage Error of the model.

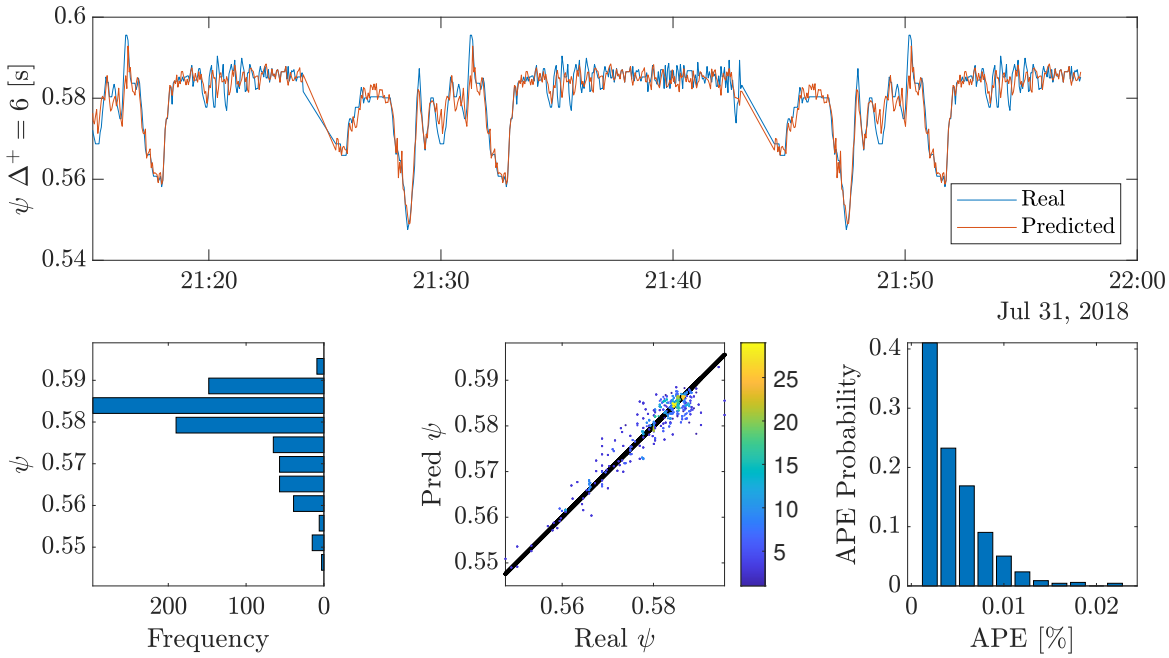

(d) The short-term motions forecasting for the trim (ψ) angle for $\Delta^+ = 6$ [s] and $\Delta^- = 15$ [s] is fixed according to Table 2. The figure includes a portion of the track in time with the real and predicted motion, the histogram of frequencies for the real motion, a heatmap scatterplot of the real versus predicted values, and a histogram of the Absolute Percentage Error of the model.

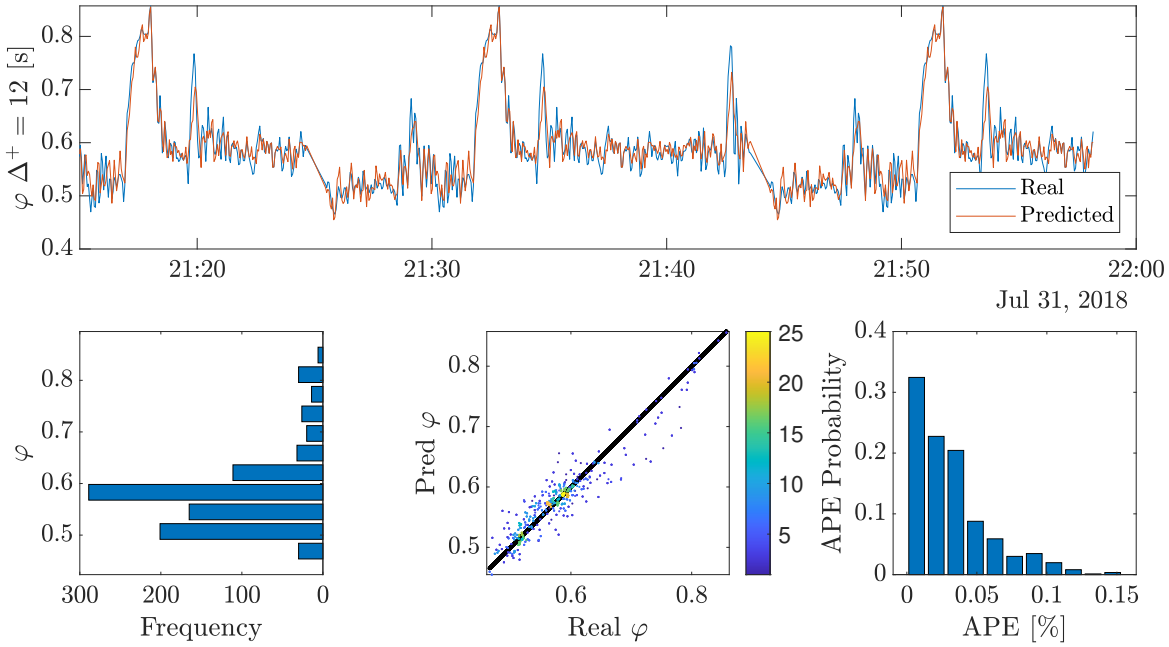

(e) The short-term motions forecasting for the roll (φ) angle for $\Delta^+ = 12$ [s] and $\Delta^- = 30$ [s] is fixed according to Table 1. The figure includes a portion of the track in time with the real and predicted motion, the histogram of frequencies for the real motion, a heatmap scatterplot of the real versus predicted values, and a histogram of the Absolute Percentage Error of the model.

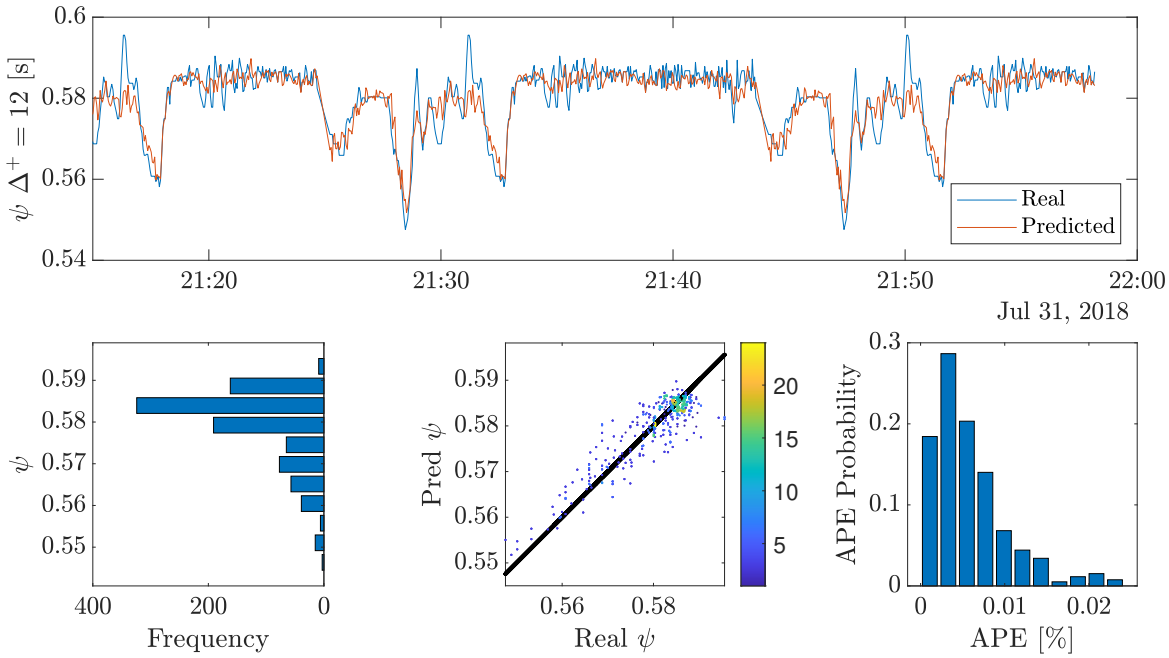

(f) The short-term motions forecasting for the trim (ψ) angle for $\Delta^+ = 12$ [s] and $\Delta^- = 15$ [s] is fixed according to Table 2. The figure includes a portion of the track in time with the real and predicted motion, the histogram of frequencies for the real motion, a heatmap scatterplot of the real versus predicted values, and a histogram of the Absolute Percentage Error of the model.

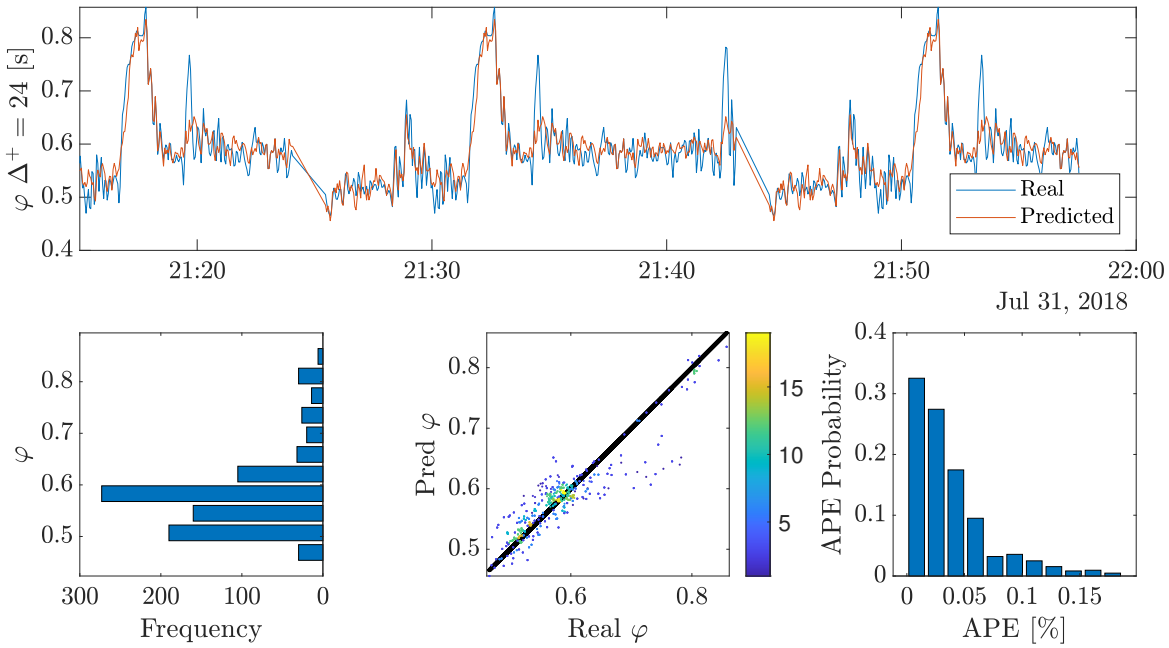

(g) The short-term motions forecasting for the roll (φ) angle for $\Delta^+ = 24$ [s] and $\Delta^- = 30$ [s] is fixed according to Table 1. The figure includes a portion of the track in time with the real and predicted motion, the histogram of frequencies for the real motion, a heatmap scatterplot of the real versus predicted values, and a histogram of the Absolute Percentage Error of the model.

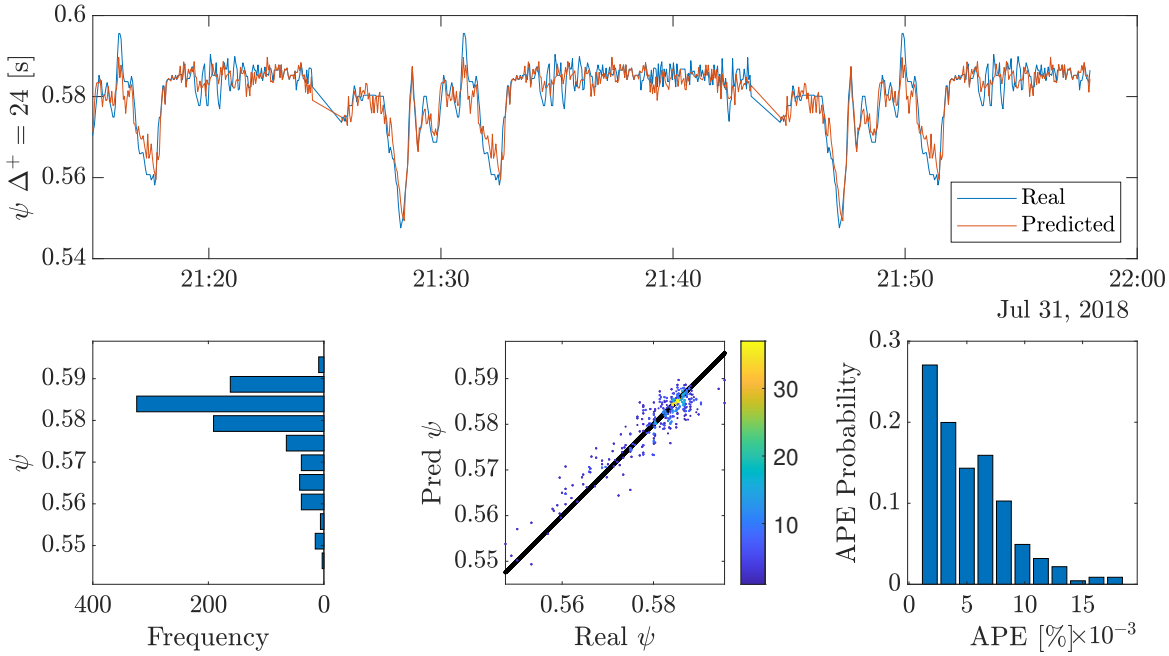

(h) The short-term motions forecasting for the trim (ψ) angle for $\Delta^+ = 24$ [s] and $\Delta^- = 30$ [s] is fixed according to Table 2. The figure includes a portion of the track in time with the real and predicted motion, the histogram of frequencies for the real motion, a heatmap scatterplot of the real versus predicted values, and a histogram of the Absolute Percentage Error of the model.

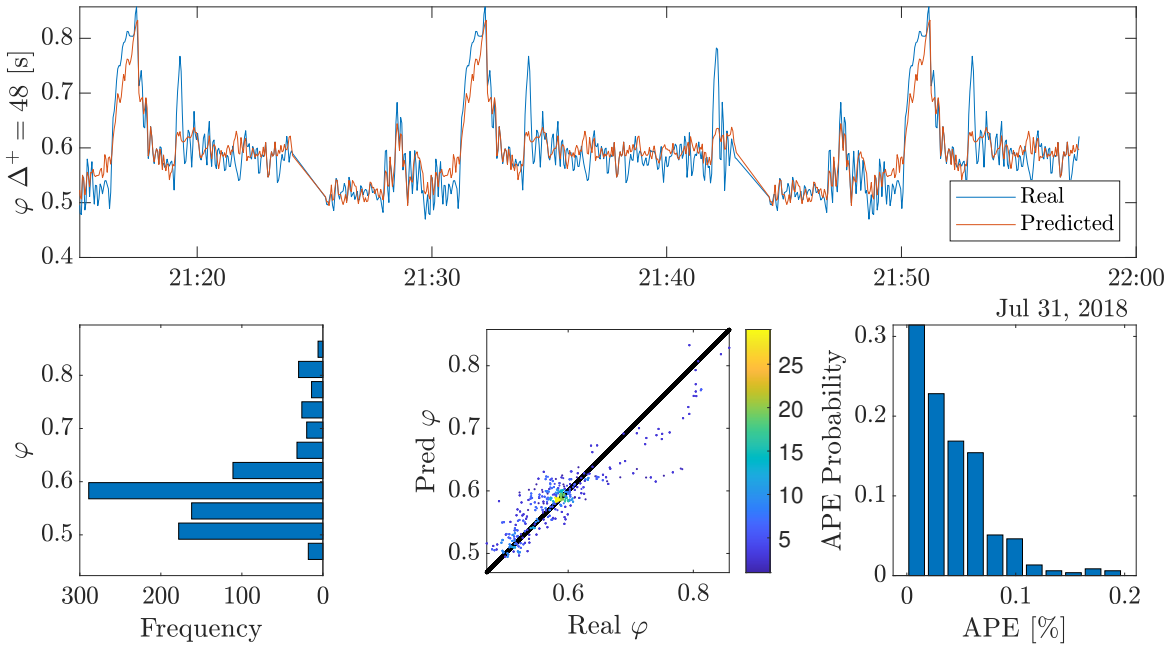

(i) The short-term motions forecasting for the roll (φ) angle for $\Delta^+ = 48$ [s] and $\Delta^- = 30$ [s] is fixed according to Table 1. The figure includes a portion of the track in time with the real and predicted motion, the histogram of frequencies for the real motion, a heatmap scatterplot of the real versus predicted values, and a histogram of the Absolute Percentage Error of the model.

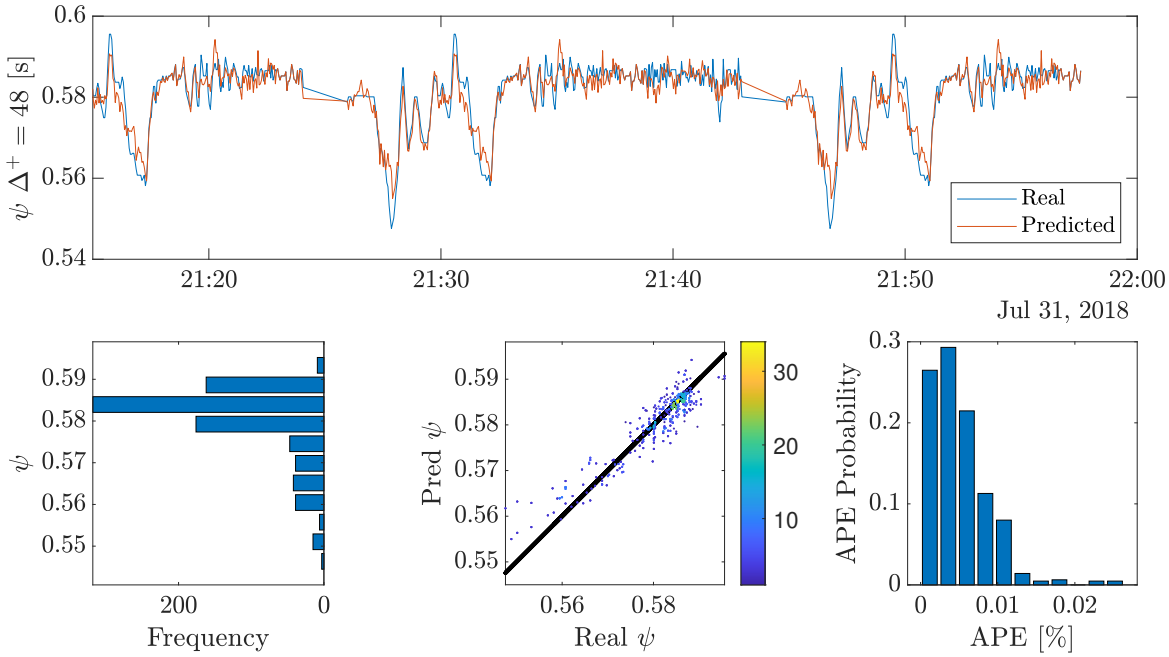

(j) The short-term motions forecasting for the trim (ψ) angle for $\Delta^+ = 48$ [s] and $\Delta^- = 30$ [s] is fixed according to Table 2. The figure includes a portion of the track in time with the real and predicted motion, the histogram of frequencies for the real motion, a heatmap scatterplot of the real versus predicted values, and a histogram of the Absolute Percentage Error of the model.

Figure 6: The short-term motions forecasting on previously unseen data for the roll (φ) and trim (ψ) angle for $\Delta^+ = \{3, 6, 12, 24, 48\}$ [s] and Δ^- fixed according to Tables 1 and 2. For each of the motions, each figure includes a portion of the track in time with the real and predicted motion, the histogram of frequencies for the real motion, a heatmap scatterplot of the real versus predicted values, and a histogram of the Absolute Percentage Error (APE) of the model.

References

Breiman, L., 2001. Random forests. Machine Learning 45, 5–32.

Coraddu, A., Kalikatzarakis, M., Walker, J., Ilardi, D., Oneto, L., 2022. Chapter 7 - Data science and advanced analytics for shipping energy systems, in: Baldi, F., Coraddu, A., Mondejar, M.E. (Eds.), Sustainable Energy Systems on Ships. Elsevier, pp. 303–349.

Coraddu, A., Oneto, L., Ilardi, D., Stoumpos, S., Theotokatos, G., 2021. Marine dual fuel engines monitoring in the wild through weakly supervised data analytics. Engineering Applications of Artificial Intelligence 100, 104179.

Cristianini, N., Shawe-Taylor, J., 2000. An introduction to support vector machines and other kernel-based learning methods. Cambridge university press.

De Masi, G., Bruschi, R., Gaggiotti, F., 2012. Short term vessel motion forecasting based on wavelet neural network for wave feed-forward dynamic positioning, in: Proceedings of the International Offshore and Polar Engineering Conference, pp. 915–919.

Fossen, T., Smogeli, Ø., 2004. Nonlinear time-domain strip theory formulation for low-speed manoeuvering and station-keeping. MIC Journal of Modeling, Identification and Control 25, 201–221.

Goodfellow, I., Bengio, Y., Courville, A., 2016. Deep Learning. MIT Press.

Hamilton, J.D., 1994. Time series analysis. Princeton university press.

International Maritime Organization, 2018. Maritime Safety Committee (MSC), 100th session, 3-7 December 2018. https://www.imo.org/en/MediaCentre/MeetingSummaries/Pages/MSC-100th-session.aspx. Last visited 11th March 2022.

Jokioinen, E., Poikonen, J., Hyvönen, M., Kolu, A., Jokela, T., Tissari, J., Paasio, A., Ringbom, H., Collin, F., Viljanen, M., Jalonen, R., Tuominen, R., Wahlström, M., Saarni, J., Nordgerg-Davies, S., Makkonen, H., 2016. Remote and Autonomous Ships - The next step. AAWA: Advanced Autonomous Waterborne Applications , 1–87.

Krishna Kumar, N., Savitha, R., Al Mamun, A., 2019. A Study on Dynamic Positioning System Robustness with Wave loads predictions from Deep Belief Network, in: Proceedings of the 2018 IEEE Symposium Series on Computational Intelligence, SSCI 2018, pp. 1520–1527.

Li, S., Fung, K.S., 2019. Maritime autonomous surface ships (mass): implementation and legal issues. Maritime Business Review 4, 330–339.

Oneto, L., 2020. Model Selection and Error Estimation in a Nutshell. Springer.

Qi, A.C., Han, Q.L., Wang, Y.L., 2015. A survey of motion control for marine vehicles. Chinese Control Conference, CCC 2015-September, 4214–4218.

Rath, B.N., Subudhi, B., 2020. An extreme learning-based adaptive control design for an autonomous underwater vehicle. volume 1. INC.

Scholkopf, B., 2001. The kernel trick for distances, in: Advances in neural information processing systems, pp. 301–307.

Shalev-Shwartz, S., Ben-David, S., 2014. Understanding machine learning: From theory to algorithms. Cambridge university press.

Shao, L., Mahajan, A., Schreck, T., Lehmann, D.J., 2017. Interactive regression lens for exploring scatter plots, in: Computer Graphics Forum.

Shawe-Taylor, J., Cristianini, N., 2004. Kernel methods for pattern analysis. Cambridge university press.

Skulstad, R., Li, G., Fossen, T.I., Wang, T., Zhang, H., 2021. A Co-Operative hybrid model for ship motion prediction. Modeling, Identification and Control 42, 17–26.

Suhermi, N., Suhartono, Prastyo, D.D., Ali, B., 2018. Roll motion prediction using a hybrid deep learning and ARIMA model. Procedia Computer Science 144, 251–258.

Thombre, S., Zhao, Z., Ramm-Schmidt, H., Vallet García, J.M., Malkamäki, T., Nikolskiy, S., Hammarberg, T., Nuortie, H., H. Bhuiyan, M.Z., Särkkä, S., Lehtola, V.V., 2022. Sensors and ai techniques for situational awareness in autonomous ships: A review. IEEE Transactions on Intelligent Transportation Systems 23, 64–83.

Vapnik, V., 1998. Statistical Learning Theory. Wiley-Interscience.

Vovk, V., 2013. Kernel ridge regression, in: Empirical inference.

Wang, L., Wu, Q., Liu, J., Li, S., Negenborn, R.R., 2019. State-of-the-art research on motion control of maritime autonomous surface ships. Journal of Marine Science and Engineering 7.

Young, D.M., 2003. Iterative solution of large linear systems. DoverPublications.

Zhang, W., Liu, Z., 2014. Real-time ship motion prediction based on time delay wavelet neural network. Journal of Applied Mathematics 2014.